Numerical study of solidifying molten metal droplet impingement on a cold solid surface

The effect of thermocapillary forces

J. W. A. Reus

Technische Universiteit Delft

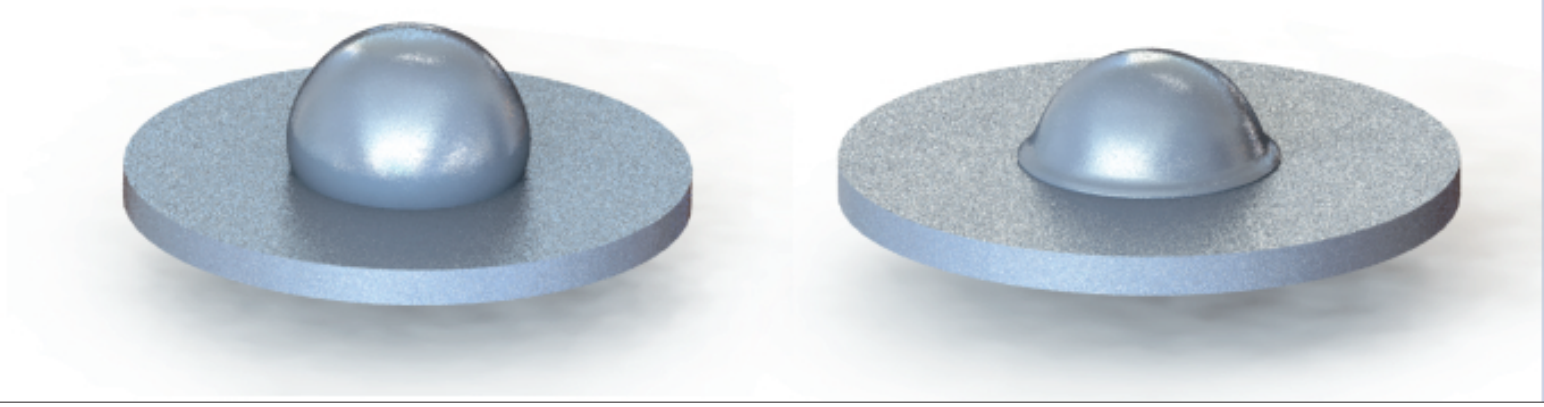

TU Delft Delft University of Technology

Challenge the future

Numerical study of solidifying molten metal droplet impingement on a cold solid surface

The effect of thermocapillary forces

by

J. W. A. Reus

in partial fulfillment of the requirements for the degree of

Bachelor of Science
in Applied Physics

at the Delft University of Technology,
to be defended publicly on Monday October 31, 2018 at 2:30 PM.

Student number:	4370465	
Thesis committee:	Prof. dr. ir. C. R. Kleijn,	TU Delft
	Dr. S. Kenjeres,	TU Delft
	Ir. A. Ebrahimi,	TU Delft

TU Delft Delft University of Technology

Abstract

Metallic droplet deposition is of interest in the industry because of the potential use in additive manufacturing. This work discusses the complex phenomena involved in droplet impingement, especially the effect of temperature dependant surface tension. The volume of fluid (VOF) method is used to solve the axis-symmetric Navier-Stokes equations, which are used to describe the droplet's behaviour. Different temperature dependencies for the surface tension are modelled, to see the effect on the interface and substrate melting. Furthermore, the effect of droplet size, initial temperature on droplet shape and substrate melting is studied.

To judge the accuracy of the VOF model, a series of benchmarks are tried. The VOF model used in this work is as accurate or more accurate than previous works.

The results show that droplets with a higher percentage of oxygen flatten, this is due to thermo-capillary forces. A higher temperature results in more spreading of the droplet, this is because higher temperatures result in higher surface tensions. These surface tensions keep the droplet together when it first makes contact with the substrate. This causes less air is trapped underneath the droplet, which causes the droplet to spread out more. The air also causes the droplet to cool down less fast, this results in a phenomenon where the hotter droplet is solidified faster than the colder one.

J. W. A. Reus
Delft, October 2018

Contents

1

Introduction

Manufacturing processes based on metallic droplet deposition are of interest in industry, such as additive manufacturing, because of the possibility of attaining desired characteristics in production by controlling and functionally grading materials. In order to achieve the desired quality in parts produced by additive manufacturing technique, optimisation and therefore understanding of solidifying molten metal droplet impingement on cold solid surfaces is required. In the pursuit of understanding of the complex phenomena involved in droplet impingement on a solid surface, a large number of analytical, experimental and numerical studies have taken place over the past few decades [1–7]. However, due to the large number of process parameters that influence the droplet behaviour, systematic studies are essential to generate a better insight into this problem. The development of computational fluid dynamics (CFD) brought an opportunity to predict the droplet behaviour during impingement and solidification that might not be achievable otherwise with the current experimental capabilities. To this end, having a model that can predict the droplet behaviour with a reasonable accuracy is critical. The objective of the present project is to investigate molten metal droplet impingement on a solid surface including phase-change (*i.e.* liquid-solid phase transformations) under the influence of thermocapillary forces.

1.1. Background and motivation

The development of additive manufacturing technology and the need to control and optimise material deposition processes have persuaded scientists to scrutinise molten metal droplet behaviour and its associated transport phenomena. A molten metal droplet carries thermal energy that can melt the substrate material during the impingement due to the energy transfer to the substrate and then re-solidifies. This, in turn, determines the mechanical and metallurgical bonding strength and the properties of constructed parts. This process strongly depends on the complex droplet behaviour and is influenced by a large number of parameters including (but not limited to) material properties, droplet and substrate temperatures and droplet velocity [3, 4, 8, 9]. Molten metal droplet deposition has been studied widely in the past decades because of its significance for both scientific and industrial applications.

Since the droplet impingement, spreading and solidification occur in a relatively short time-scale and small length scales, it is quite challenging to fully understand the underlying physics of transport phenomena through experimental investigations [10, 11]. Additionally, due to the lack of transparency of the materials that are generally used in additive manufacturing, tracking the dynamic solid-liquid interface position and the fluid flow inside the molten material is difficult or even impossible with the current experimental capabilities [10–12]. Hence, numerical simulations can be considered as an alternative to investigate the droplet behaviour to gain an insight into the mechanisms that govern the shape of a solidified droplet.

Harlow and Shannon [13] developed a numerical model for the droplet impingement on a solid surface using a "Marker-and-Cell" (MAC) technique based on the finite difference method. This two-dimensional model could track the position of marker particles by solving the fluid continuity and momentum equations. However, they simplified the problem by neglecting the effects of surface tension

and fluid viscosity, which is valid when these forces are negligible in comparison with inertial forces (*e.g.* high-speed droplets and early stages of the droplet impingement). This model has been developed latter by Tsurutani *et al.* [14] to take the viscous and surface tension effects and the heat transfer from a hot substrate to a cold liquid droplet into consideration. Handling topological changes using the MAC technique and controlling the marker distribution are problematic and increases computational costs. Due to the large deformation of the droplet during impingement on a solid surface and possibly droplet splashing and breakup at high speeds, applications of the interface tracking [13, 14] and the interface fitting [15, 16] (*i.e.* the Lagrangian formulation of the Navier–Stokes equations using moving meshes) methods are limited for these type of problems. To overcome the limitations associated with interface tracking and interface fitting methods, interface capturing methods such as Volume of Fluid (VOF) [17] and Level-Set (LS) [18] methods have been applied extensively to study the droplet behaviour [19–23].

The droplet will cool down due to heat diffusion towards the substrate, which results in the droplet solidification, hence a solidification model is needed.Madejski [24] took the solidification and melting process into consideration to model the impingement and solidification of a droplet. Kamnis and Gu [25] utilised the porosity technique that uses a momentum sink term to model the solidification of a droplet. Besides solidification, surface tension and impact velocity are important parameters that determine the shape and behaviour of an impinging droplet, [11, 26]. Surface tension of a liquid can vary with temperature and concentration of active elements. Temperature gradients induced at the droplet-substrate interface during deposition process result in a change in surface tension and cause Marangoni-driven flows. Marangoni flow can influence the droplet in several ways. Monti *et al.* [27] noticed a reduction in wetting of silicone droplets on a horizontal flat substrate, which is caused by Marangoni velocities at the free surface. Cao *et al.* [28] states that solutal Marangoni convection is critical in solidification processes, leading to local concentration changes in alloys. Increased melting rates in molten droplets has been observed by Khodadadi [29], this was due to temperature-induced Marangoni convection. Song [30] studied the internal droplet flow numerically and stated that the flows are often dominated by surface tension forces, instead of buoyancy forces. The authors of previous works explicitly stated that Marangoni convection has a significant influence on the fluid dynamics of the molten droplet. One of these previous works is the work of Dietzel *et al.* [31] which also portrays the importance of the Marangoni convection. In his research the surface tension is taken into account, however, it is assumed to be linear negative dependant on temperature. This means that when the temperature rises, the surface tension is getting lower.

In the present work, the surface tension will be modelled more realistically, with both negative and positive surface tension gradients. These surface tension gradients are more likely to occur in practical applications. In addition, Dietzel's did not simulate the substrate remelting. However, as is stressed by Braun *et al.* [32], the substrate temperature influences the spreading and thus the shape of the droplet. Therefore, substrate remelting is also taken into consideration in the present study.

The aim of this project is to investigate the effects of thermocapillary forces on molten metal droplet behaviour during impingement and its shape after solidification on a solid cold and flat surface.

1.2. Research Question

The research question that will be answered in this thesis is: "What are the influences of thermocapillary forces on a molten metal droplet during impingement on a cold flat solid surface?". A secondary question that will be answered is: "what is the size of the liquid pools formed due to substrate melting caused by a molten metal droplet impinging on a substrate". To study these problems, a numerical approach is utilised. Simulations are carried out to investigate the influence of droplet size, droplet initial temperature, and the active element concentration. Validity and reliability of the VOF solver and the numerical models employed in the present study are also examined for different benchmark cases.

1.3. Outline

This thesis is organised as follows: Chapter two consists of the problem description, mathematical models,boundary conditions and numerical methods used to simulate the droplet impingement. Chapter three contains the test cases which are used to validate the mathematical model and the solver. Four known benchmark test cases which asses relevant physical aspects are reported as well. The grid and domain size study are discussed in chapter three. The fourth chapter discusses the results of the droplet impingement and substrate bonding. Chapter five ends this thesis with the concluding commentary as well as recommendations for future studies and the limitations of the present study.

2

Theoretical model

2.1. Problem description

The schematic of the studied physical problem is shown in figure 2.1. A molten metal droplet with a diameter of l and an initial temperature T_{d} is impinging on a horizontal flat substrate with a velocity v. Gravity is acting on the droplet and pulls it into the direction of the substrate. The initial substrate and surrounding air temperature is 300K. The material used for the substrate and droplet are the same. Thermo-physical properties of the material can be found in table 2.1. T_{d} is higher than the melting temperature of the metal used, T_l. Oxygen is used as the active element in the molten iron droplet influencing the temperature dependence of the surface tension. The substrate has an initial temperature of T_s. In the model, different values are chosen for $l, T_{\mathrm{d}} - T_{\mathrm{l}}$ and the active element concentration to be able to see their effect on the shape of the impinging droplet and substrate melting. The thickness of the substrate is 3.5 mm and the size of the domain will be L. The size of the domain is determined in the domain size study in chapter 3.3. The domain is axisymetric.

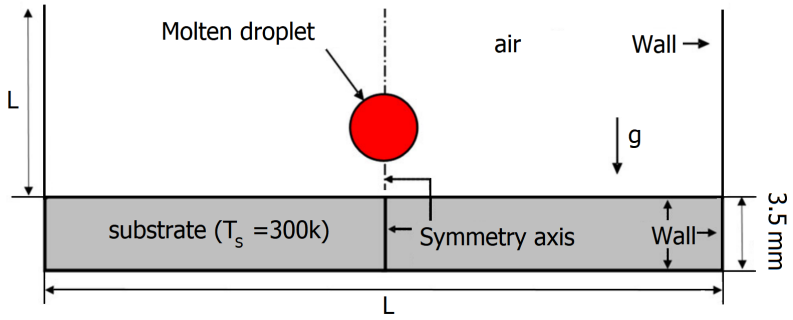

Figure 2.1: This figure shows the computational geometry and boundary conditions for the simulation of droplet impingement and solidification.

Table 2.1: Material properties of the droplet impinging on a solid surface and the substrate.

Property/parameter	Value	Unit
density, ρ	7200	$\mathrm{kg \cdot m^{-3}}$
dynamic viscosity of molten metal,μ	0.006	kg(m· s)$^{-}$1
Solidus temperature,T_{sol}	1697	K
Liquidus temperature, T_{l}	1727	K
Specific heat capacity, c_{p}	712	$\mathrm{J(kg \cdot K)^{-1}}$
Thermal conductivity of solid material	15	$\mathrm{W(m \cdot K)^{-1}}$
Thermal conductivity of molten material	33	$\mathrm{W(m \cdot K)^{-1}}$
Latent heat of fusion, h	2.47×10^5	$\mathrm{J \cdot kg^{-1}}$

2.2. Mathematical models and boundary conditions

The governing equations for the incompressible solid-liquid-gas model are the continuum equations of the conservation of mass, momentum, and energy.

mass conservation:

$$\nabla \cdot (\vec{u}\rho_{\text{eff}}) = 0, \tag{2.1}$$

momentum conservation:

$$\frac{\partial \rho_{\text{eff}}\vec{u}}{\partial t} + \rho_{\text{eff}}(\vec{u}\cdot\nabla)\vec{u})) = \nabla[-p + \mu_{\text{eff}}(\nabla\vec{u} + (\vec{u})^{\text{T}})] + \overrightarrow{F_{\text{st}}} + \rho_{\text{eff}}\vec{g} + S_{\text{m}}, \tag{2.2}$$

energy conservation:

$$\frac{\partial \rho_{\text{eff}}H}{\partial t} + \nabla \cdot (\rho_{\text{eff}}\vec{u}H) = \nabla(k_{\text{eff}}\nabla T) + S_{\text{T}}, \tag{2.3}$$

Where, $\vec{u}$ is velocity, $\vec{g}$ gravitational acceleration , ρ effective density, t time, μ effective dynamic viscosity, F_{st} surface forces, H enthalphy, k effective thermal conductivity, S_{m} the solidification source therm and S_{T} the energy source therm which accounts for latent heat. Both these formulas are conservation equations for two-phase flow. The only difference with a single-phase flow is that ρ and μ are discontinuous and the momentum equation has an additional therm to take surface tension into consideration[33].

To model the solidification and melting, a liquid fraction parameter is introduced, f_{l}. The melt interface is implicitly represented by f_{l} and is based on the enthalphy-prososity method. f_{l} is equal to zero if the temperature of the control volume is equal to or below the solidus temperature. If the temperature of the cell reaches a temperature higher than the liquidus temperature, f_{l} will be 1. Values between one and zero represent the mushy zone, where both liquidus and solid phases are present.

$$f_{\text{l}} = \begin{cases} 0 & \text{if } T < T_{\text{solidus}} \\ 1 & \text{if } T > T_{\text{liquidus}} \\ \frac{(T - T_{\text{solidus}})}{(T_{\text{liquidus}} - T_{\text{solidus}})} & \text{if } T_{\text{solidus}} < T < T_{\text{liquidus}} \end{cases} \tag{2.4}$$

The enthalpy-porosity method treats the mushy zone as a porous medium. When the temperature decreases, the liquid fraction will decline. The latent heat formed by the solidification will dissipate. The energy source therm S_{T} accounts for this latent heat. S_{T} is equal to:

$$S_{\text{T}} = -\left[\frac{\partial \rho \Delta H}{\partial t} + \nabla \cdot (\rho u \Delta H)\right] \tag{2.5}$$

where Δ H is expressed as:

$$\Delta H = \beta L, \tag{2.6}$$

L is the latent heat of the material in liquid phase. With this information the total enthalpy of the material is calculated by adding the sensible enthalpy h and the latent heat ΔH:

$$H = h + \Delta H \tag{2.7}$$

where

$$h = h_{\text{ref}} + \int_{T_{\text{ref}}}^{T} C_{\text{p}} dT, \tag{2.8}$$

h_{ref} represents the reference enthalpy at the temperature T_{ref}. C_{p} stands for the specific heat of the material.

If the liquid fraction of a computational cell is equal to zero, the velocities of that cell will also become zero. This is expressed in the momentum equation as the source term S_{m}[34]:

$$S_{\mathrm{m}} = \frac{(1-f_{\mathrm{l}})^2}{(f_{\mathrm{l}}^2+\epsilon)} C_{\mathrm{mush}} \vec{u} \tag{2.9}$$

C_{mush} is the mushy zone constant and a higher mushy zone constant means a higher dampening of velocity of the solid. ϵ is a small constant here chosen to be 0.001. In this work C_{mush} is equal to 10^{10}, as suggested by Zheng *et al.* [35].

2.2.1. Surface tension model

Active element concentration and temperature both influence the surface tension. The relation between these parameters and the surface tension had been described by Belton [36]. The subject has been studied by Sahoo *et al.* [37] for several materials. The surface tension σ is expressed as

$$\sigma = \sigma_{\mathrm{m}}^0 - A(T-T_m) - RT\Gamma_s \ln\left[1+Ka_{\mathrm{i}}\right], \tag{2.10}$$

where

$$K = k_1 e^{-\frac{\Delta H^0}{RT}} \tag{2.11}$$

The surface tension of a pure metal at melting temperature T_{m}, is depicted as $\sigma_{\mathrm{m}}^0 = 1.943\ \mathrm{Nm}^{-1}$. R is the gas constant, T is the temperature, A is the negative temperature coefficient of surface tension and is equal to $4.3\times10^{-4}\mathrm{Nm}^{-1}\mathrm{K}^{-1}$ for pure iron, $k_1 = 1.38\times10^{-2}$ which is constant and related to the segregation entropy, a_{i} is the activity of species i dissolved in the solution, $\Gamma_s = 2.03\times10^{-8}\mathrm{Mol\ m}^{-2}$ is the surface excess concentration at saturation and the standard heat of absorption for the iron-oxygen system is $\Delta H^0 = -1.463\mathrm{J\ Mol}^{-1}$.

When eq. 2.10 is differentiated with respect to temperature, γ is obtained, which is the temperature coefficient of surface tension. γ is a function that is both dependent on the temperature and oxygen activity a_{i}:

$$\gamma = -A - R\Gamma_s \ln\left[1+Ka_{\mathrm{i}}\right] - \frac{Ka_{\mathrm{i}}}{1+Ka_{\mathrm{i}}}\frac{\Gamma_s \Delta H^0}{T} \tag{2.12}$$

When γ is positive the fluid will flow from colder regions towards hotter regions due to the thermo-capillary effect. If γ is negative there will be a reverse flow motion. This means that changes in temperature or oxygen concentration in the molten metal droplet can result in flow reversal, when the changes results in an sign change of γ. For pure liquid iron this is not possible as γ can not be positive.

When oxygen is added to the system, γ will first be positive at lower temperatures and above a certain temperature γ will be negative. The flow reversal will occur at the maxima of the surface tension, when γ is zero. The temperature coefficient and surface tension for the iron-oxygen system can be seen in figure 2.2. The temperature range shown in this figure is 1800-3000 K.[38]

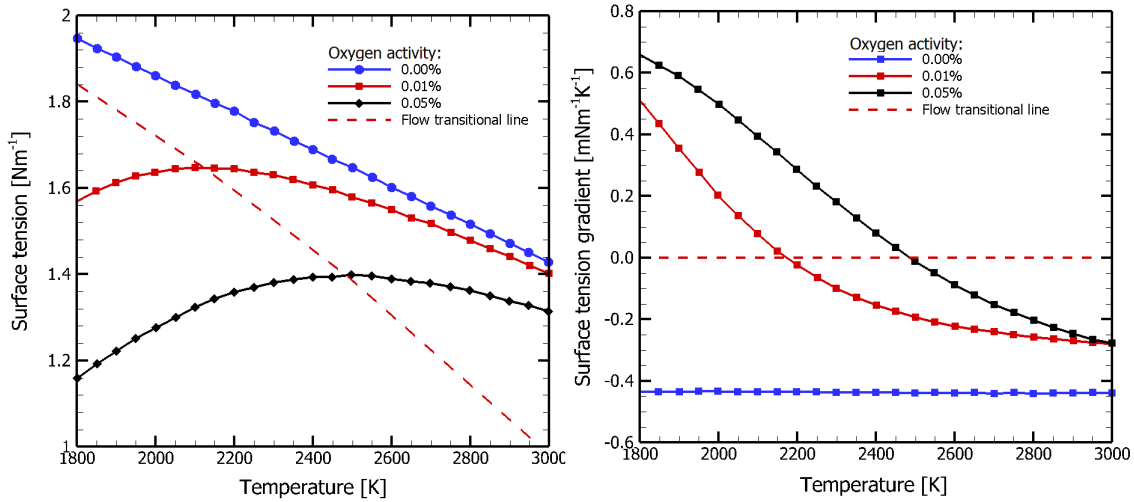

Figure 2.2: The left image shows the surface tension dependence on temperature for different oxygen levels. The right image shows the surface tension gradient dependance on temperature for different oxygen levels.

The numerical method used in this work (VOF) requires the surface force to be a volumetric surface force $\mathrm{F_s}$, while surface forces act only on the surface. To transform the surface force per unit area f_s into a volumetric surface a Delta function is used:

$$\mathrm{F_s} = f_\mathrm{s}\delta = f_\mathrm{s}|\nabla\zeta| \tag{2.13}$$

Where ζ is only non-zero for interface cells. The surface force per unit area is composed of normal and tangential components. The tangential component depends on the surface tension gradient, the normal component is determined by the local value of surface tension and the curvature of the interface. As can be seen in the following formula

$$f_\mathrm{s} = f_\mathrm{s,n} + f_\mathrm{s,t} = \sigma\kappa\vec{n} + \nabla_\mathrm{t}\sigma \tag{2.14}$$

n is equal tot the surface normal vector, ∇_t is the tangential gradient operator and κ is the curvature defined as:

$$\kappa = -(\nabla\cdot\vec{n}) \tag{2.15}$$

and $\vec{n}$ is defined as

$$\vec{n} = \frac{\nabla\zeta}{|\nabla\zeta|} \tag{2.16}$$

The tangential componen is experessed as:

$$\nabla_\mathrm{t}\sigma = \gamma\nabla_\mathrm{t}T = \gamma[\nabla T - \vec{n}(\vec{n}\cdot\nabla T))] \tag{2.17}$$

If these equation are combined it yields:

$$\mathrm{F_s} = [\sigma\kappa\vec{n} + \gamma(\nabla T - \vec{n}(\vec{n}\cdot\nabla T))]|\nabla\zeta| \tag{2.18}$$

This method is proposed by Brackbill *et al.* [39].

The importance of the surface tension gradient due to thermal-capillary effects compared to the viscous forces is given by the Marangoni number(Ma) [40, 41].

$$\mathrm{Ma} = \frac{\gamma L \Delta T}{\mu \alpha} \tag{2.19}$$

Where γ is the gradient of surface tension compared to temperature, ΔT the temperature gradient, μ the dynamic viscosity and L the chosen length scale in this work the droplet diameter. α is the thermal diffusivity and is formulated as follows:

$$\alpha = \frac{k}{\rho c_{\mathrm{p}}} \tag{2.20}$$

For a high Marangoni number, $\mathrm{Ma} \geq 80$, the effect of surface tension can not be neglected.[42] The absolute Marangoni number chosen in this work will be between $0.66 \cdot 10^5$ and $1.07 \cdot 10^5$.
A temperature gradient in the droplet also leads to a density gradient, which induces buoyancy effects that might influence the shape of the droplet. However, the Marangoni flow is much more decisive compared to the buoyancy flow. This is represented by a small dynamic bond number which is the ratio of the Rayleigh and Marangoni number:

$$\mathrm{Bo} = \frac{\mathrm{Ra}}{\mathrm{Ma}} = \frac{\rho g \beta T L^3/(\mu\alpha)}{\gamma L \Delta T/(\mu\alpha)} = \frac{\rho g \beta L^2}{\gamma} \tag{2.21}$$

Where β is the thermal expansion coefficient, which is $11 \cdot 10^{-6}\mathrm{K}^{-1}$. This ratio is in the order of 10^{-2} - 10^{-3} as a result of the small diameter of the droplets. Because of this it can be assumed that buoyancy is negligible compared to the Marangoni effect.

Boundary conditions

The boundary condition on the outer walls are as follows: the boundaries have a no slip condition and are at a constant temperature of 300K. The substrate wall has a no slip boundary as well, and a thermal contact resistance of $1.8 \cdot 10^{-6}\ \mathrm{m}^{-2}\ \mathrm{K}\ \mathrm{W}^{-1}$, as is proposed by Kamnis and Gu [25]. The dynamic viscosity is assumed to be constant. Dietzel *et al.* [31] shows that the effect of temperature on the dynamic viscosity is negligible.

There are different wall-impingement regimes (*i.e.* splash, induced breakup, breakup, boiling, spread, stick, rebound and rebound with breakup). These criteria depend on the Reynolds number, Weber number and initial temperature. The Weber number is the ratio of the fluid's inertia compared to the its surface tension and is defined as:[43]

$$\mathrm{We} = \frac{\rho v^2 L}{\sigma} \tag{2.22}$$

Where σ is the surface tension and v is the velocity of the droplet. The contact angle of the droplet is assumed to be constant. This can be done because the weber number is below 30[31]. For the droplet's Weber number to be below 30, a initial droplet velocity of 1.25 ms^{-1} and a initial droplet diameter of below 3mm is chosen. The Reynolds number is the relative importance of the inertial forces of the fluid compared to the viscous forces and is defined as[43]:

$$\mathrm{Re} = \frac{\rho v L}{\mu} \tag{2.23}$$

Because the Renolds number in our problem is low it can be assumed that, the molten droplet and surrounding air is incompressible and the flow is laminar. The wall temperature is 300K and it has a no slip boundary, *i.e.* the velocity at the walls is zero. A two-dimensional axi-symmetric domain has been used for modelling the impingement and solidification of a molten metal droplet.

2.3. Numerical methods

ANSYS Fluent which is a commercial flow solver, is used in the present study to simulate molten droplet impingement and solidification. The simulations are executed in parallel on 16 cores. Surface tracking is done using the volume of fluid (VOF) method.

2.3.1. Volume of fluid method

To track the droplet interface, the volume of fluid (VOF) method is used. This technique was first Proposed by Hirt in 1979[17]. The idea of the VOF method is to assign each cell a value that is defined as the volume fraction of the fluid within each cell. A gas filled cell will have a value of zero while a liquid filled cell will have a value of one. The VOF method is an "one" fluid method, this means that a single set of conservation equations (2.2, 2.1) needs to be solved for every cell. If only this method is applied, the interface will be a blurred region. To determine the actual interface, one needs to first find cells with a value between 0 and 1. An example of this can be seen in figure 2.3. If these cells are identified one should determine the interface by analysing the volume fraction in the neighbouring cells.[33, 44].

To be able to retrieve the interface from the scalar field two approaches can be applied: interface-reconstruction and interface-sharpening. Interface-reconstruction is an explicit method, while interface-sharpening is implicit. Geometric reconstruction is an example of an interface-reconstruction scheme. Compressive interface capturing scheme for arbitrary meshes (CICSAM) is an interface-sharpening scheme. Several schemes will be assessed using a benchmark case to determine the most accurate one for this work. These schemes are CICSAM, compressive, geo-reconstruc and modified-HRIC and are explained in the ANSYS User's Guide [45].

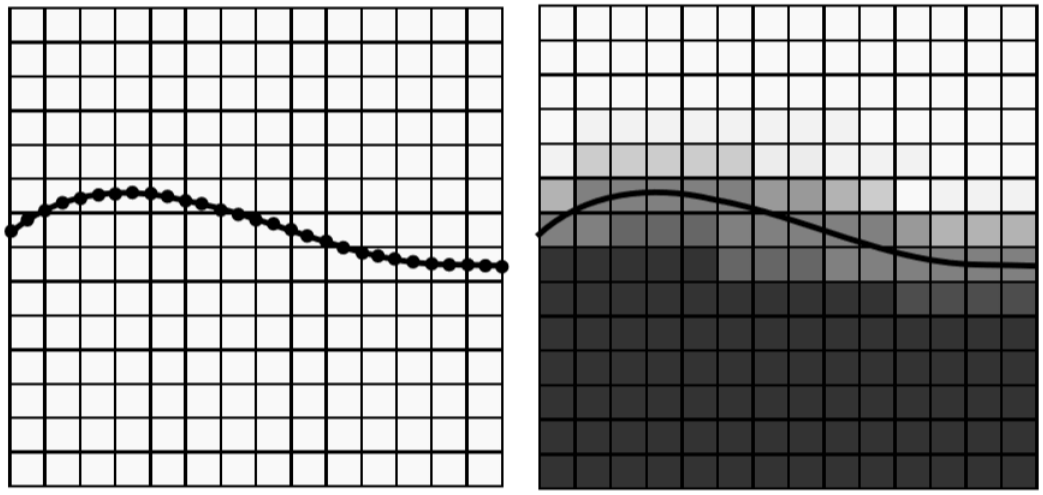

Figure 2.3: The left image shows the initial liquid-air interface. The right image shows what the VOF uses to calculate the next time step. To retrieve the left image out of the right image a interface-reconstruction scheme is needed.

The position of the moving interface is computed by solving the volume fraction continuity equation for the liquid phase:

$$\frac{\partial F}{\partial t} + \nabla \cdot \vec{u}F = 0 \tag{2.24}$$

With F defined as:

$$F = \frac{\text{Surface of a cell occupied by fluid}}{\text{Surface area of the cell}} \tag{2.25}$$

With the use of the volume fraction, volume-fraction-averaged material properties can be given as

$$\rho = F\rho_{\mathrm{l}} + (1 - F)\rho_{\mathrm{g}} \tag{2.26}$$

$$k_{\mathrm{eff}} = Fk_{\mathrm{l}} + (1 - F)k_{\mathrm{g}} \tag{2.27}$$

$$c_{\mathrm{eff}} = Fc_{\mathrm{l}} + (1 - F)c_{\mathrm{g}} \tag{2.28}$$

$$\mu_{\mathrm{eff}} = F\mu_{\mathrm{l}} + (1 - F)\mu_{\mathrm{g}} \tag{2.29}$$

Where properties with the subscript l are liquid and g are gas properties. The effective material properties are the ones used in equation 2.1, 2.2 and 2.3. The VOF algorithm is devided in two parts, a propagation and reconstruction step. The orientation of the interface is determined during the reconstruction step. It is used to determine the unit normal vector $\vec{n}$. The next step is propagation, this is done using an operator split method or fractional step which updates F by calculating the governing equations one dimension at a time. The intermediate F values are calculated, the final volume fraction is obtained after advection of the interface along the two directions (x, y).

2.3.2. Level-set method

The level set (LS) method is used to model incompressible two phase flows. This method is able to capture the interface between two fluids by considering a scalar function, ψ, which is continuous and smooth. ψ is equal to zero when at the interface, it is positive in one phase and negative in the other. The function is initialised as the signed minimum distance function with relation to the interface, which means $|\nabla\psi| = 1$. After a time step the function need to be re-initialised, at that moment $|\nabla\psi|$ is only true at the interface. The progression of the level set function, when the interface is influenced by an external velocity field is defined as:

$$\frac{\partial\psi}{\partial t} + u \cdot \nabla\psi = 0 \tag{2.30}$$

The progression of ψ uses the same conservation equations as the VOF method (2.1,2.2,2.3). When using LS the material properties are described as follows:

$$\rho(x,t) = \rho_{\mathrm{g}} + (\rho_{\mathrm{l}} - \rho_{\mathrm{g}})H_\epsilon(\psi(x,t)) \tag{2.31}$$

$$k_{\mathrm{eff}}(x,t) = k_{\mathrm{g}} + (k_{\mathrm{l}} - k_{\mathrm{g}})H_\epsilon(\psi(x,t)) \tag{2.32}$$

$$c_{\mathrm{eff}}(x,t) = c_{\mathrm{g}} + (c_{\mathrm{l}} - c_{\mathrm{g}})H_\epsilon(\psi(x,t)) \tag{2.33}$$

$$\mu_{\mathrm{eff}}(x,t) = \mu_{\mathrm{g}} + (\mu_{\mathrm{l}} - \mu_{\mathrm{g}})H_\epsilon(\psi(x,t)) \tag{2.34}$$

$H_\epsilon(\psi(x,t))$ denotes the smoothed Heaviside function. The discontinuous Heaviside function causes numerical instability, because of this the smoothed Heaviside function is used, as first proposed by Sussman *et al.* [46]. The smoothed Heaviside function:

$$H_\epsilon(\psi) = \begin{cases} 0 & \text{if } \psi < -\epsilon \\ 1 & \text{if } \psi > \epsilon \\ \frac{\psi+\epsilon}{2\epsilon} + \frac{\sin(\pi\psi/\epsilon)}{2\pi} & \text{if } |\psi| \leq \epsilon \end{cases} \tag{2.35}$$

ϵ is a value chosen to be one to two times the local mesh size and represents half the interface thickness. The Continuum Surface Force model (CSF) of Brackbill *et al.* is used to approximate the surface tension therm F_{s} used in equation 2.2.

$$F_{\mathrm{S}} = \sigma k(\psi)\mathbf{n}\delta_\epsilon(\psi) \tag{2.36}$$

Where σ the surface tension coefficient, $k(\psi)$ is the mean curvature of the surface, $\delta_\epsilon(\psi)$ smoothed delta function defined as the partial derivative of $H_\epsilon(\psi)$ with respect to ψ and $\mathbf{n}$ the normal vector of the surface, and defined as:

$$\mathbf{n} = \frac{\nabla\psi}{|\nabla\psi|} \tag{2.37}$$

and

$$k(\psi) = \nabla \cdot \frac{\nabla\psi}{|\nabla\psi|} \tag{2.38}$$

The level set function ψ stops being a signed distance function to the interface after the first time step integration. This is a problem that can be solved by reinitializing ψ regularly. Preferred is to initilialize ψ at every time step [46]. Further information can be found in [33].

2.3.3. Coupled level-set and volume of fluid model

The normal of the surface can be accurately calculated using the level set method. However, this method is found to be inadequate in preserving volume conservation [47]. When the VOF method is used, the volume is conserved due to the tracking of the volume fraction instead of the interface itself. The downside of using the VOF method is the inability to calculate the spatial derivatives due to its discontinuous surface. To be able to use the advantages of both methods a coupled level-set and VOF method is provided in ANSYS Fluent.

The level-set function is unlikely to maintain the distance constraint of $|\nabla\psi| = 1$. This is caused by the deformation of the interface, thickness across the interface and uneven profile. The errors will accumulate after each iteration and will cause intolerable large errors in the mass, momentum and energy solutions. The process needs to be re-initialized after each time step, to do this the geometrical interface-front construction method is used. The procedure is as follows:

1. Find the cells where the value of the volume fraction is between zero and one or where the sign of ψ is alternating. These cells are partially filled and contain the interface.
2. Use the level-set function to calculate the normal of the interface for each interface cell.
3. Make sure that at least one corner of the cell contains the designated phase with regard of the neighbouring cells and position the cut-through.
4. Find the intersection of the cell centre line normal and the interface, in such a way that the VOF is satisfied.
5. Find the intersection points of the interface line and the cell boundaries. The intersecting points are designated as the front points.

Now the interface front is reconstructed, the procedure can begin for the minimisation of the distance from the interface to a given point.

1. The distance of each cut segment of the interface cell to the a given point is calculated. The distance calculation method is as follows:
   (a) When the normal line from the given point to the interface intersects within the cut-segment, the calculated distance will be the distance to the interface.
   (b) When the normal line from the given point to the interface-intersect is not withing the cut-segment, the calculated distance will be the distance from the point to the intersection of the cell and interface.
2. These distances are minimised from the given point to all interface cut-segments. The values of these distances will be used to re-initialize the level-set function.

2.3.4. Spatial discretization

To solve the governing equations the computational cell face values are required, as well as their gradients. The VOF method only depend on variables that are stored and calculated at the cell centres. Interpolation of the cell centre values is used to express the cell face values. The interpolation technique used in this work is Central Differencing Scheme (CDS) for the momentum and energy equation. Other schemes that are commonly used by other studies are Upwind Differencing Scheme (UDS) and Quadratic Upwind (QUICK), more information about these schemes can be found in [41].

Central Differencing Scheme

The Central Differencing Scheme (CDS) works as follows. The cell face value ϕ_f is approximated by linearly interpolating between two neighbouring cell centres who share the same face f.

$$\phi_f = \phi_A \lambda_f + \phi_D (1 - \lambda_f) \tag{2.39}$$

where

$$\lambda_f = \frac{x_f - x_D}{x_A - x_D} \tag{2.40}$$

Cell n is defined as the acceptor cell with centre value ϕ_A and n+1 as the donor cell with ϕ_D as can been seen in figure 2.4. *x* indicates the coordinate of the value that is considered. CDS is second order accurate and is thus non-diffuse. However, the results obtained using this method are unbound. Meaning that the solution oscillates, especially when simulating problems dominated by convection. This means that CDS will generally be able to retain the sharpness of the interface. However, because it is unbounded the scheme will often give unphysical results when used for interface sharpening. [48]

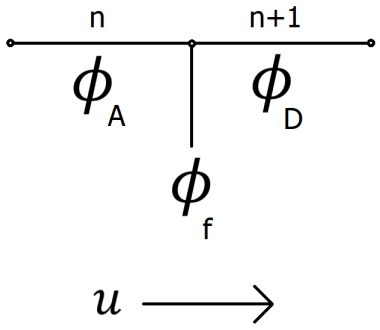

Figure 2.4: Indication of the donor and acceptor cell. In between the donor and acceptor cell is the face value. The arrow indicates the flow direction.

2.3.5. Temporal Discretization

This work makes use of transient simulation, which means that the governing equation must be discretized. The discritization of time involves the integration of every single term in the differential equations over time Δt. The transient terms are integrated as follows:

$$\frac{\partial \phi}{\partial t} = F(\phi) \tag{2.41}$$

Where $\frac{\partial \phi}{\partial t}$ is a generic expression for the time evolution and F embodies any spatial discretization. In this work first-order discretization is used

$$\frac{\partial \phi}{\partial t} \approx \frac{\phi^{m+1} - \phi^{m}}{\Delta t} = F(\phi) \tag{2.42}$$

Where m is the value at the current time and $m+1$ is the value at $t+\Delta t$. $F(\phi)$ needs to be evaluated, this can be done implicit or explicit. In this work the implicit time integration is used because of the advantage that it remains stable for large time steps. Another reason that is chosen for the implicit time integration is that when working with incompressible flows the solution must be iterated to converge within each time step. The equation for implicit time integration

$$\phi^{m+1} = \phi^{m} + \Delta t F(\phi^{m+1}) \tag{2.43}$$

3

Results

In this chapter all the results will be presented. This includes the results of the validation cases, grid study and domain study. It also include the results of the impinging droplet with solidification case with different initial parameters, to see the effect of these parameters on the droplet interface and liquid pool of the substrate.

3.1. Code validation and verification

This chapter shows the results of the validation cases and compares these with experimental or analytic data. Three aspects will be validated with three different cases. To validate the free surface tracking, a dam break problem is used. For the validation of the solidification process, an one dimensional solidification benchmark problem is used. To consider phase change, heat transfer and fluid flow in a single benchmark, a thermo-capillary flow with phase change benchmark is numerically modelled.

3.1.1. Dam break Case

To confirm the VOF free surface tracking, the two-dimensional dam break case is used. This problem is the standard validation case for the CFD simulations that include gravity flows[49]. The problem consists of a rectangular water column situated on the left side of a container. A more detailed description can be seen in figure 3.1. At $t = 0$ the water column is released and begins to flow due to gravity forces. The dimensionless time used for the dambreak case is as follows $t^* = t\sqrt{\frac{g}{a}}$, where $a = 0.1$m

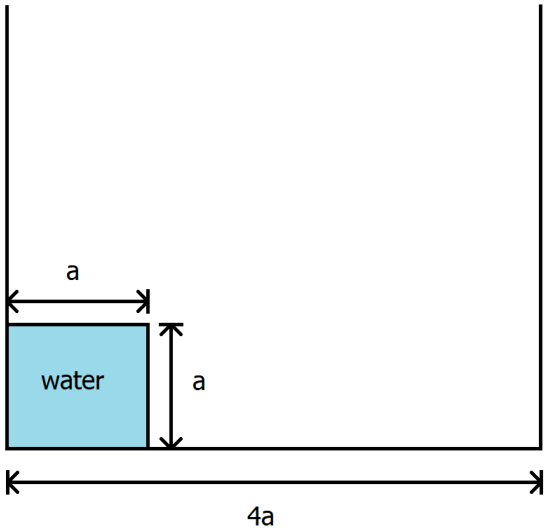

Figure 3.1: Two dimensional dam break, geometry of the problem. In the simulation done by the present study $a = 0.1$m.

A square water column with sides $a = 0.1\mathrm{m}$ is used in this case. More details of this case can be found in the work of A. Vorobyev [49]. The results of the several free surface reconstruction methods are depicted in figure 3.2. These results are compared with both experimental results of Martin and Moyce [50] as numerical results from Ketabdari *et al.* [51]. Figure 3.2 shows the propagation of the water front compared with time. The distances is scaled by the initial distance of a and t^* is the dimensionless time.

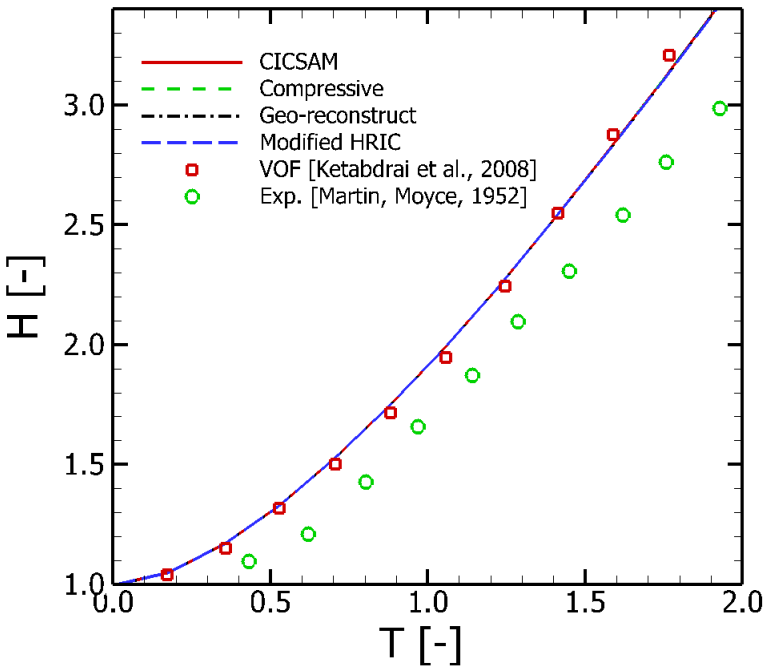

Figure 3.2: Position of the waterfront compared to non-dimensional time T for the dam break experiment. This figure shows the different numerical schemes compared to experimental data [50].

The difference between the different free surface reconstruction methods is negligible. The numerical studies show a difference with the experimental results. This is probably due to aspects that are not considered in the numerical studies. For example, the resistance of the ground acting upon the water is not modelled. Another aspect is the breaking of the dam, the experimental study physically removed a dam, this slows the propagation of the waterfront. This is not modelled in the numerical studies. Therefore the compressive method is chosen, because it takes the least computational time.

The difference between the dambreak case with level set and without level set are shown in figure 3.3. In this case the compressive method is used as interface sharpening method for the VOF.

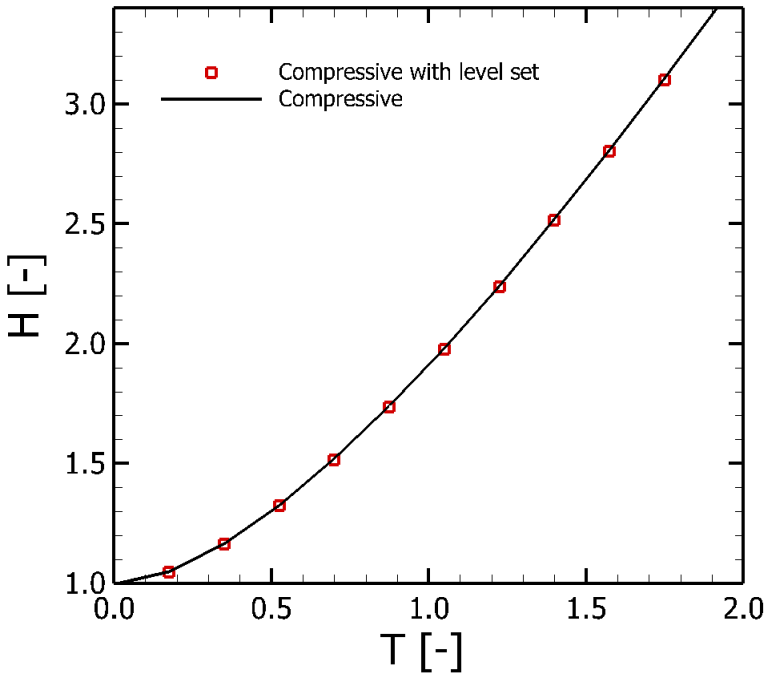

Figure 3.3: Position of the waterfront compared to non-dimensional time T for the dam break experiment. This figure shows the difference of using the VOF method compared to the coupled level set with VOF method

The difference between the VOF method and the CLS method is negligible and the CLS method requires more computational time, thus the VOF method is chosen to model the impinging droplet.

3.1.2. 1D solidification benchmark

The benchmark problem is used to validate the solidification model. This problem consists of a one-dimensional slab of Al-Cu alloy. The alloy with 4,5% Cu has an uniform temperature of 969K at the start of the problem, resulting in a molten alloy, because the liquidus temperature is 919k. The left wall of the slab is set to a fixed temperature of 573K. This temperature is below the solidus temperature of 821K. Fluid flows are not considered in this benchmark problem. The distance of the liquidus and solidus lines from the left wall are tracked and compared with semi-analytical and numerical result. These results are presented in figure 3.4.

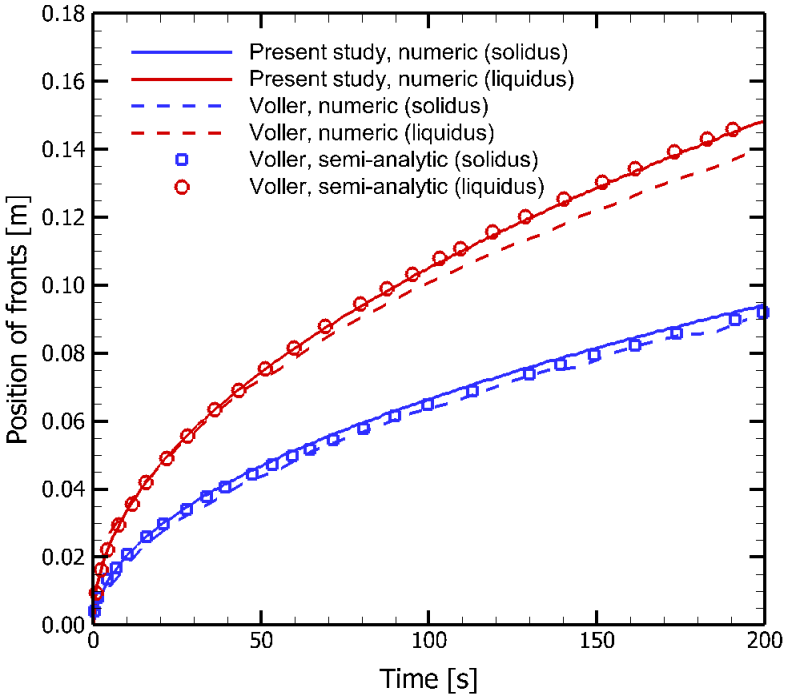

Figure 3.4: One-dimensional solidification benchmark, position of liquidus and solidus front over time. Both semi-analytic as numeric results from Voller and Swaminathan [52], compared to results from present work.

One can see that the results from the present study are closer to the semi-analytic data than the numerical results of Voller and Swaminathan [52].

3.1.3. Thermocapillary driven flow with phase change

Heat transfer, fluid flow and phase change are considered in a benchmark by melting bismuth below an argon gas layer. A slot is modelled numerically up to steady state. The slot is initially filled with two-thirds (10mm) liquid and one-third solid bismuth(5mm), with a height of 4mm. The right wall of the slot has a temperature below melting point while the left wall has a temperature above the melting point of bismuth. The top and bottom boundaries have a linear temperature distribution, pinning the solid-liquid interface to the initial position where the temperature is equal to the melting temperature. The system is placed in a microgravity environment. More information about the benchmark can be found in the work of Tan *et al.* [53]. The schematics of the case can be seen in figure 3.5.

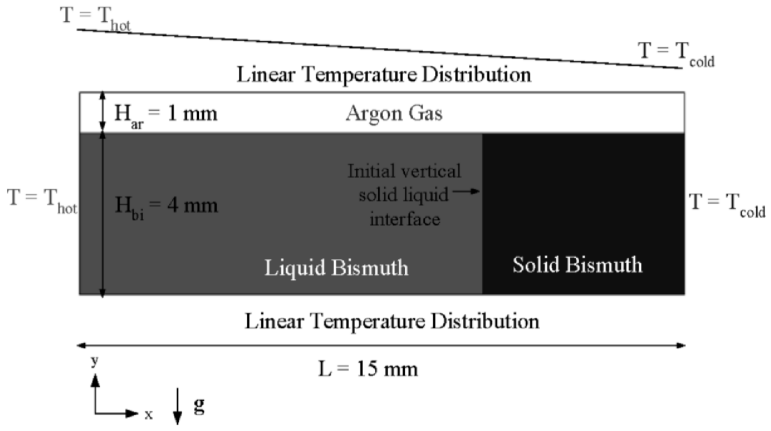

Figure 3.5: Problem setup of the thermocapillary dirven flow with phase change case by Tan *et al.* [53]

The solid-liquid interface that is obtained from the present solver is compared to numerical reference data [41, 53, 54].

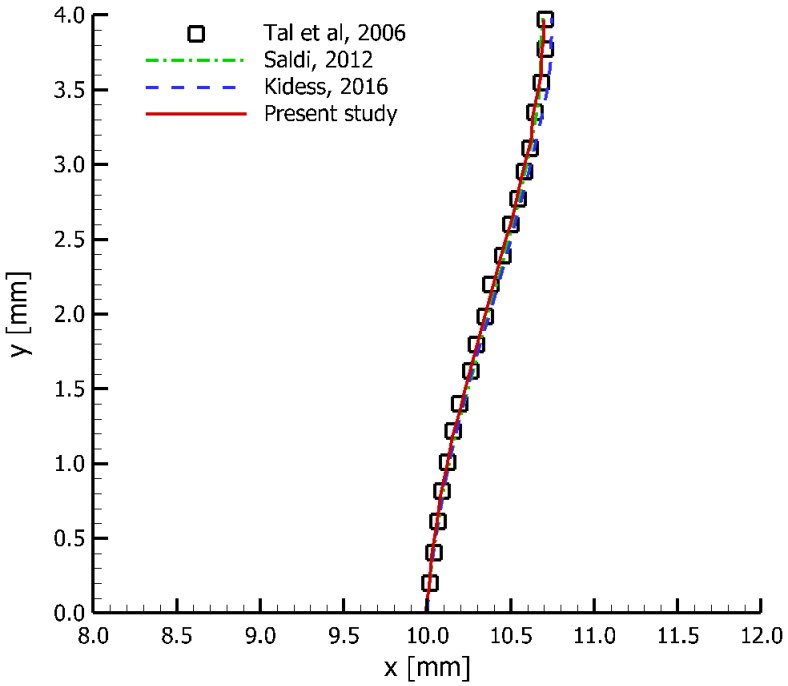

Figure 3.6: Position of the solid-liquid interface of the thermocapillary driven flow case at steady state. This figure shows the data of several numerical studies compared to the data retrieved from the solver of the present work

The difference between the different cases is negligible. This means that it can be assumed that the numerical model used in the present study correctly models thermocapillary flow, fluid flow, phase change and heat transfer.

3.1.4. Droplet impingement

Droplet impingement and solidification is modelled and compared to experimental data to see if the model used in this work is true to nature. A molten tin droplet initially has a temperature of 513 K, the melting temperature of tin is 505 K. The initial diameter, D_0 is 2.7 mm and the droplet has a velocity of $1 ms^{-1}$. The substrate consists of stainless steel initially at 298 K with an thermal contact resistance of $5 \cdot 10^{-6} m^2 K W^{-1}$ Initial conditions and other parameters are taken from experimental reference work.[4] Figure 3.7 shows the spreading over time after the droplet impinges on a substrate. The spreading is mad dimensionless by dividing through the initial droplet diameter. This is compared with both an experimental as an numerical study. [4, 55]

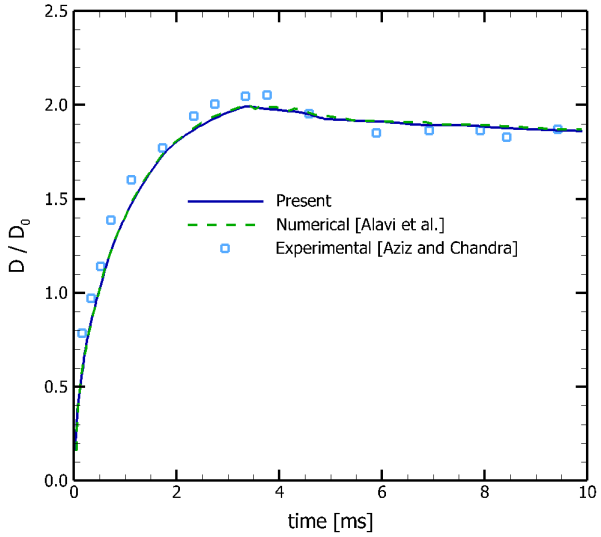

Figure 3.7: This figure shows the droplet spreading over time. Both an experimental and numerical study is shown to be able to compare it with results from the present work.

The difference between the present numerical study and the numerical study of Alavi is negligible. There is a difference with the experimental study this is due to factors that are not taken into account in the numerical studies. For example, it is assumed that the contact angle is a constant at $140°$. This is not the case in an actual experiment.

3.2. Grid study

To make sure that the results are independent of the computational grid size, multiple grid sizes are examined. The smearing of the interface should not influence the surface forces. To see if the grid size has an effect on the droplet behaviour, the maximum droplet diameter after solidification is checked. The parameters to compare are non-dimensional quantities, D/D_0 is the maximum droplet diameter after impingement divided by the initial droplet diameter. $\Delta x/D_0$ is the computational cell length divided by the initial droplet diameter. The case used for the grid study is the same case as depicted in the problem description. A molten steel droplet lands on a colder substrate and solidifies. The droplet has an initial temperature of 750K above liquidus temperature and an oxygen activity of 0.05%. The droplet diameter is 3.0mm.

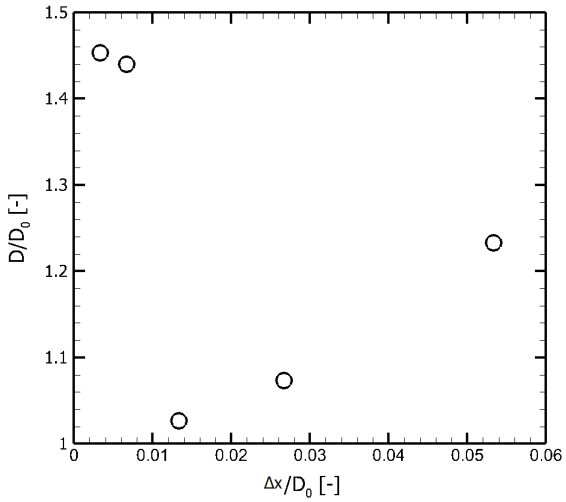

Figure 3.8: This figure shows the computational grid size and droplet diameter after solidification, respectively Δx and D. The parameters are both made dimensionless by dividing by the initial droplet diameter, D_0

At a grid size of 20 μm the air underneath the droplet at impingement is correctly modelled, this is not the case at 40 μm and causes the jump at 40 to 20 μm. The difference between 10 and 20 μm is negligible. Because of this a grid size for the fine grid is 20 μm. Another reason for the choice of making the grid size 20 μm, is the calculation time. A case with a 10 μm grid takes two times as long as a case with a 20 μm grid.

3.3. Domain size study

The results should not be influenced by the size of the computational domain. The wall boundaries on the ceiling and the side walls need to be at such a distance that the walls do not have any effect on the air currents generated by the droplet. Furthermore, the domain needs to be of such size that the droplet does not heat the whole domain, this can have an effect on the solidification process of the droplet. To see if the domain size influences the droplet, the diameter of the droplet is compared for different domain sizes. The domain size represents both the height and the width of the domain. The case used to determine the domain size is the same case used to determine the grid size and can is described in chapter 2.1. The droplet has an initial temperature of 750K above liquidus temperature and an oxygen activity of 0.05%. The droplet diameter is 3.0mm.

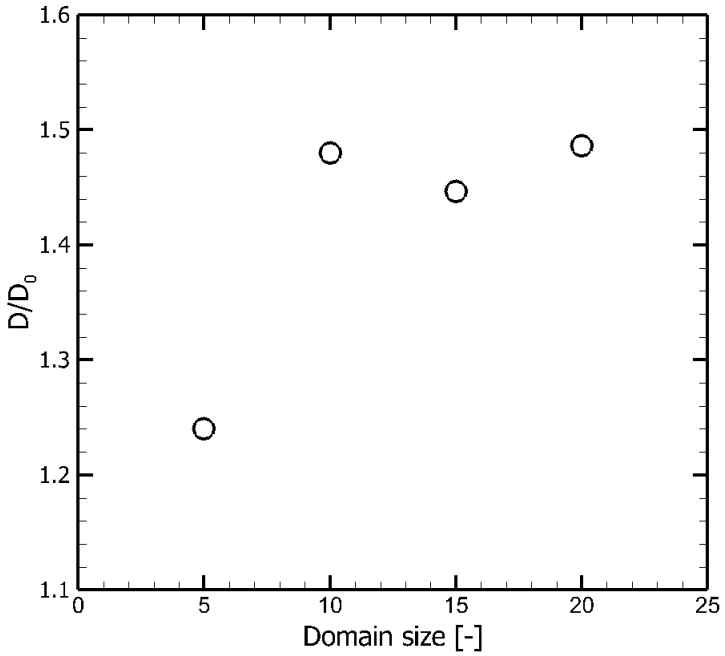

Figure 3.9: The domain size compared to the spreading of the droplet both made dimensionless by dividing by the initial droplet size. The domain size represents both the height and the width of the domain.

It can be seen that the droplet radius is constant when the domain size is equal or larger than 10 times the diameter of the droplet. The domain size does not influence the computational time much, because only the coarse mesh region gets larger. Because of this the amount of computational cells does not increase much when choosing a larger domain. For further work a domain size of 15 times the droplet diameter is chosen to make sure the result is domain size independent.

3.4. Results of droplet impingement with substrate remelting

In order to investigate the effects of temperature, oxygen level and size on droplet impingement and solidification behaviour, the interface of the droplet as well as the liquid pool size of the substrate are shown in this chapter. But first the droplet impingement progress is shown.

3.4.1. Droplet impingement process

The images are subtracted from the case where the initial temperature is 750K above the liquidus temperature, the oxygen activity is 0.05% and the initial droplet diameter is 3.0 mm.

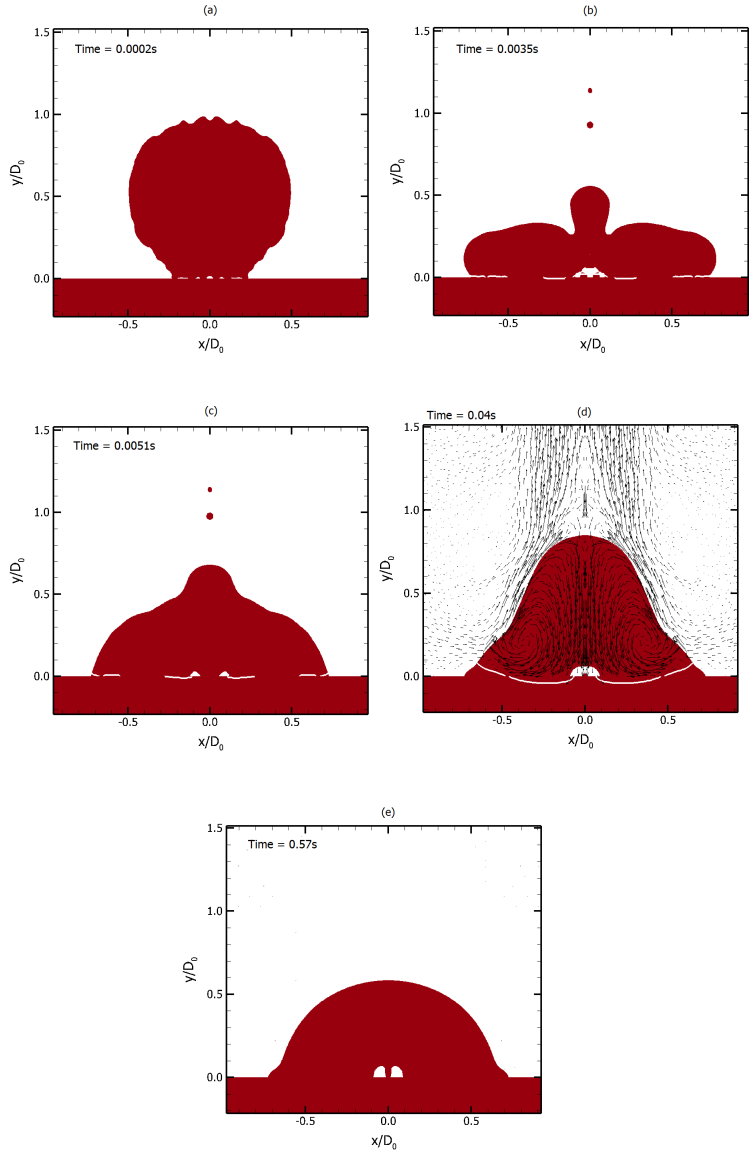

Figure 3.10: (a)Impinging droplet on a cold surface. The axis are made dimensionless by dividing by the initial droplet diameter of 3.0mm.(b) Spreading of a molten metal droplet on a cold surface. The white line shows the liquid-solid interface.(c)This figure shows the recoil of an impinging droplet. After it hits the surface and spread the droplet recoils as can be seen here. (d) Droplet impinged on cold substrate at t = 0.04s. The vectors show the velocities of the droplet. (e) Solidified liquid metal droplet after impinging on a cold substrate.

The droplet impinges on the surface after release and traps some air underneath, as can be seen in figure 3.10 (a). The amount of air trapped underneath a droplet is different for each case, for example the droplet impingement for the case where $\Delta T = 250K$ is shown in figure A.3, and shows a larger amount of air trapped. After impinging the droplet spreads because of the inertia forces and gravity. This can be seen in figure 3.10 (b).

The diameter of the droplet is largely determined at this phase and only the shape of the droplet will change. After the spreading of the droplet, the surface tension pulls the droplet back into a spherical shape. The recoil can be seen in figure 3.10 (c). The spreading and recoiling happens a few times, as the surface forces are converted into inertia and then back to surface forces. This movement is damped, because of internal resistance. When the inertia is damped sufficiently thermocapillary forces become dominant. When the inertia forces is damped the thermocapillary and surface tension become the dominant forces. This can be seen in figure 3.10 (d). It can be seen that the Marangoni effect causes a flow, upward towards the hot region and back through the middle due to gravity. This causes a fortex that seem to bring hot fluid towards the colder substrate. The droplet begins to solidify and at t = 0.57s the droplet is fully solidified, as can be seen in figure 3.10 (e).

3.4.2. Temperature

Three different initial temperatures of 750, 500 and 250K above liquidus temperature (1727K) are chosen for the droplet. Figure 3.11 shows the interface of the droplet after solidification with different initial temperatures. The oxygen activity is 0.05% and the initial droplet size is 3.0mm.

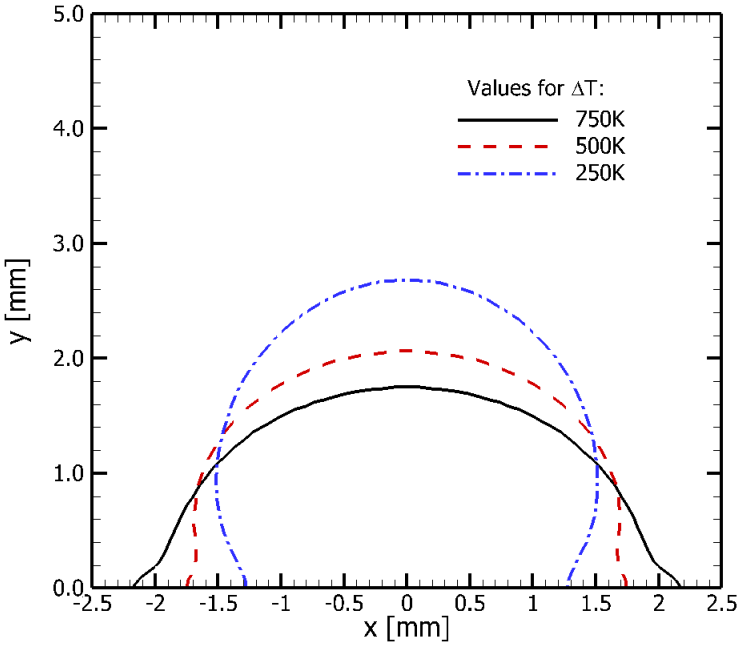

Figure 3.11: Interface of solidified droplet after impinging on a solid surface with different initial temperatures. Where ΔT is equal to the initial temperature minus the liquidus temperature of the droplet.

A higher temperature shows a larger droplet diameter after solidification. The effect of the temperature on the liquid pool size in the substrate can be seen in table 3.1.

Table 3.1: Different liquid pool size parameters compared to different initial temperatures. Where ΔT is equal to the initial temperature minus the liquidus temperature of the droplet. The maximum substrate melt pool depth is D_m, W_m is the maximum melt pool width and A_m the maximum cross sectional area. t_m is the time that the maximum melt area is achieved.

ΔT [K]	750	500	250
D_m [mm]	0.13	0.061	0.0
W_m [mm]	2.4	1.3	0.0
A_m [mm^2]	0.13	0.092	0.0
t_m [s]	0.035	0.040	-

The interfaces of the droplet at maximum melting area are shown in figure A.2. The maximum velocity at the interface at t = 0.04s is 0.76 ms^{-1}.

3.4.3. Oxygen level

The oxygen level determines the behaviour of the surface tension gradient, which in turn has an effect on the shape of the droplet. This can be seen in figure 3.12 where the interface of an impinging droplet is shown after solidification with different oxygen activities.

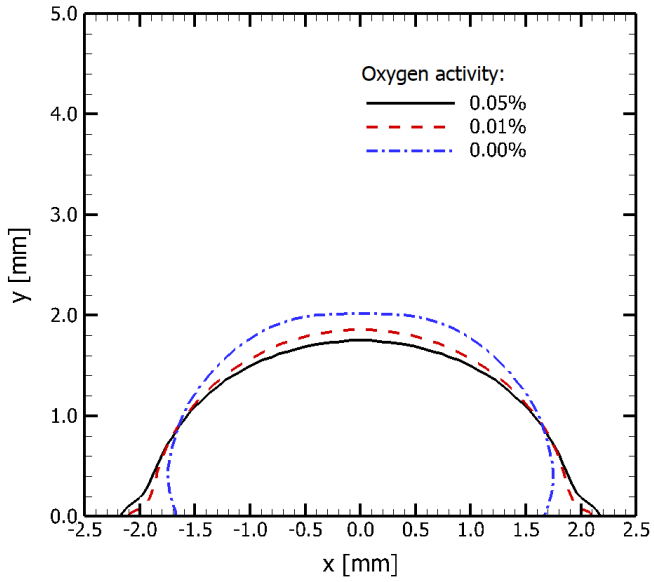

Figure 3.12: This figure shows the interface of an impinged metal droplet after solidification. The different lines indicate different oxygen levels in the droplet.

A negative surface tension gradient results in a smaller diameter of the droplet, compared to a positive surface tension gradient. The negative surface gradient is due to an oxygen percentage of 0 in the droplet. While the positive and partly positive surface tension gradient is caused by an oxygen level of 0.01 and 0.05%. To see the effect of different oxygen levels on substrate melting, one should look at table 3.2.

Table 3.2: Different liquid pool size parameters compared to different oxygen percentages in the droplet. The maximum substrate melt pool depth is D_m, W_m is the maximum melt pool width and A_m the maximum cross sectional area. t_m is the time that the maximum melt area is achieved.

Oxygen level [%]	0.05	0.01	0.00
D_m [mm]	0.13	0.083	0.052
W_m [mm]	2.4	1.2	0.68
A_m [mm^2]	0.13	0.18	0.076
t_m [s]	0.035	0.054	0.057

The interfaces of the droplet at maximum melting area are shown in figure A.1. The maximum velocity at the interface at t = 0.04s is 0.76 ms^{-1} for the 0.05% oxygen case. For the 0.01% case this is at the exact same time 0.70 ms^{-1}.

3.4.4. Droplet size

The interface of an impinging droplet with different initial sizes is shown in figure 3.13. The axis are scaled to the radius after impinging, *i.e.* X* and Y* is equal to the actual droplet size divided by the droplet diameter of that droplet after solidification.

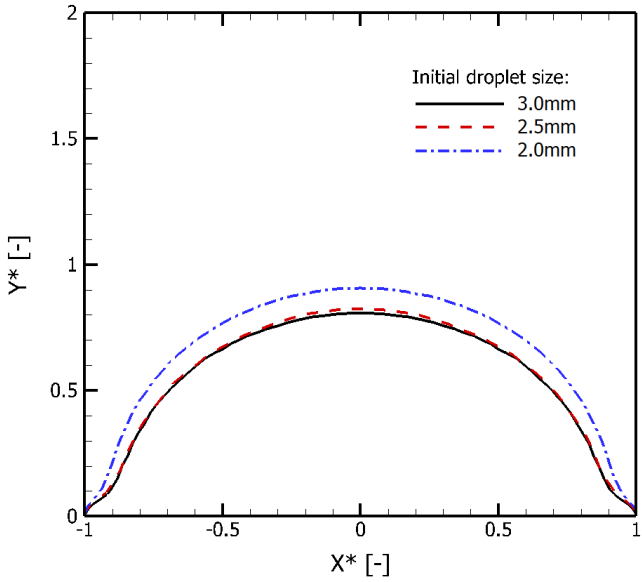

Figure 3.13: The interface of impinged metal droplets on a solid surface after solidification. The different lines indicate different initial droplet sizes. Both axis are made dimensionless by dividing by the maximum spreading of the droplet after solidification.

It can be seen that an initial droplet size of 25 and 30 mm give an identical droplet shape, while an initial droplet size of 20 mm shows a different droplet shape. The effect of the initial droplet size on the liquid pool size in the substrate can be seen in table 3.3.

Table 3.3: Different liquid pool size parameters compared to different initial droplet diameters. The maximum substrate melt pool depth is D_m, W_m is the maximum melt pool width and A_m the maximum cross sectional area. t_m is the time that the maximum melt area is achieved.

Initial droplet diameter [mm]	3.0	2.5	2.0
D_m [mm]	0.13	0.10	0.081
W_m [mm]	2.4	2.1	1.78
A_m [mm^2]	0.13	0.096	0.074
t_m [s]	0.035	0.026	0.019

4

Discussion

4.1. Droplet shape

Both the oxygen level and initial temperature influence the shape of the solidified droplet considerably. The initial droplet diameter mostly influences the droplet diameter after solidification but not the shape of the droplet, as can be seen in figure 3.13. Increasing the initial temperature and thus the Marangoni number, flattens the droplet and increases spreading. This behaviour is also observed by Dietzel *et al.* [31]. This is because of the initial surface tension difference. The droplet with lower temperatures also have a lower surface tension. When the droplet first hits the substrate the bottom is pushed upwards and sideways. At low initial temperatures this causes a protrusion near the interface, as can be seen when comparing figure 3.10 and A.3. This protrusion is allowed to be formed due to the low surface tension and creates an air bubble. At higher surface tension the protrusion is much smaller and thus traps less air underneath the droplet. This trapped air influences the shape of the droplet and the solidification. The diameter of the droplet is already determined after the first spreading and before the first recoil. At this moment inertia and surface tension forces are dominant. This means that thermocapillary forces have a small influence on the spreading of the droplet.

After the inertia is damped the surface tension and thermo capillary forces are the dominant forces. At this phase both the droplet with 0.01 and 0.05% oxygen have a positive surface tension gradient, due to the lower temperature. This means that the Marangoni flow of the 0.01% case, although smaller, has the same direction as the 0.05% oxygen case. The reason the 0.01% case has a smaller diameter than the 0.05% case is because of the smaller Marangoni number, which results in a smaller flow away from the substrate. The case of 0.00 % oxygen has a smaller spreading than the other cases, this is due a change in direction of the Marangoni flow. The flow is directed towards the colder surface, in the other cases it is directed away from the surface. The change is caused by the negative Marangoni number which is a result of the negative surface tension gradient.

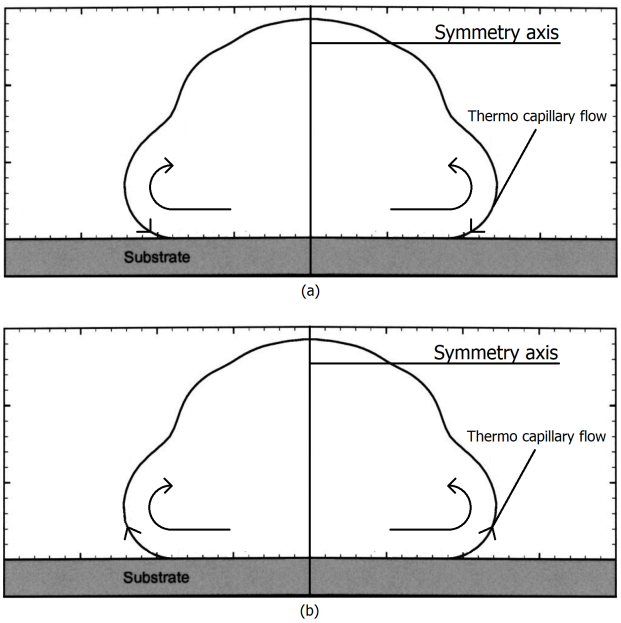

Figure 4.1: (a) shows the negative γ case where there is a higher surface tension at lower temperatures. This causes a flow towards the substrate. (b) shows the positive γ case where there is a higher surface tension at high temperatures forcing the a flow away from the substrate.

The flow directed away from the substrate, increases the spreading. While flow towards the substrate limits the ability to spread. This is because the flow towards the substrate counteracts the inertia forces in the beginning of the droplet impingement. However, the most dominant factor that determines the shape is the surface tension and inertial forces of the impinging droplet. A droplet with a higher surface tension tends to be more spherical, while a droplet with a lower spreads more. This can be seen in the different oxygen cases. The case with the lowest oxygen percentage and highest surface tension, has the most spherical shape and least spreading. Increasing the oxygen level and thus lowering the surface tension makes the droplet spread more.

4.2. substrate bonding

When lowering the initial temperature of the droplet the size of the liquid pool in the substrate also decreases, this is because the droplet has less energy to heat the substrate. At a ΔT = 250K, the temperature of the droplet is not high enough to be able to melt the substrate. Another reason why the substrate does not melt in the lower temperature region, is because a bigger air droplet is trapped underneath the droplet compared to the higher initial temperatures, this can be seen comparing **??** with A.4. This droplet prevents a part of the droplet from touching the substrate, which results in a lower heat flux. Because of the lower heat flux, the droplet with the initial lower temperature solidifies slower, as can be seen in figure 4.2. A_1 is the area of the droplet above the melting temperature and A_0 is the initial area above melting temperature.

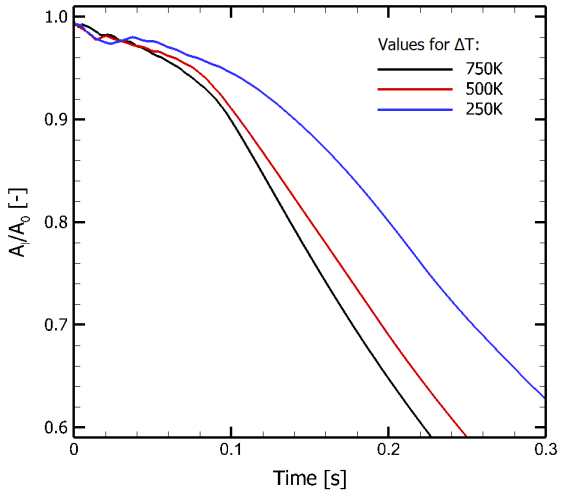

Figure 4.2: This figure shows the solidification over time, where A_1 is the cross sectional area of the droplet above the melting temperature and A_0 is the initial cross sectional area above melting temperature. This case has an active element concentration of 0.05% and an initial size of 3.0mm

When increasing the temperature the pool depth increases, both due the fact that a droplet with higher temperature has more energy to melt the substrate and the heat transfer from droplet to substrate is faster which makes it easier to overcome the heat dissipation of the substrate.

Smaller droplets create smaller liquid pools in the substrate. This is because smaller droplets have less energy to melt the substrate. However, the smaller droplets liquid pools are equal or larger, in proportion to diameter of the initial droplet size. The smaller droplets can melt the substrate more easily, because the heat is more concentrated on a single spot. The small melt pool and lower energy reserve of smaller droplets result in quicker resolidification of the melt pools, which can be seen in the lower time it takes to reach the largest melt pool.

The difference in maximum melt area achieved time for the different oxygen cases is due to the Marangoni effect. A higher Marangoni effect creates more internal flow, because of this flow more hot fluid is directed towards the substrate and increases the heat flux. This increases the pool depth and width considerably. But also causes the droplet to cool down and solidify faster.

5

Conclusion

This chapter contains a concluding commentary as well as recommendations for future studies and the limitations of the present study.

5.1. Conclusions

A numerical study was presented, studying the effects of initial droplet size, temperature and oxygen level on the shape and substrate melting of impinging metal droplets. Different sizes of the initial droplet do not effect the shape of the droplet, only the size when impinged. Oxygen levels do effect the droplet shape, however it has been found that this is mostly due to surface tension differences and not due to thermocapillary forces. Temperature also effects the shape of the impinging droplet significantly. A lower initial temperature causes the droplet to be more spherical because of the initial lower surface tension. This initial lower surface tension causes a protrusion near the surface, which creates an air bubble and limits the droplet spreading.

The substrate melting is enhanced with higher Marangoni number, this is due to a higher refresh rate of fluid near the substrate. This enhances the substrate melting but also causes the droplet to solidify faster. Lower initial temperature causes the substrate to melt less. However, because of the air bubble formed by the low surface tension, the lower temperature droplets solidify slower. Smaller droplets solidify faster due to having less initial energy compared to bigger droplets.

5.2. Recommendations and future works

This work has given insight on what effect the thermo-capillary forces have on the shape of the droplet, and how it influences the substrate melting. However, everything is assumed to be axis-symmetrical. The forming of the air bubble and the substrate melting can be influenced by this assumption. To see if this is the case a three dimensional numerical should be made and used to check if the three dimensional model gives different results compared to this work. This thesis also showed that surface tension is an important factor for the solidified droplet shape. Future work could look into the droplet-substrate bonding after solidification. Questions regarding the strength of the bonding can be answered, for instant, what the effect of the trapped air bubble has on substrate bonding. This can also help additive manufacturing by optimising the temperature for optimal bonding strength.

A

Appendix

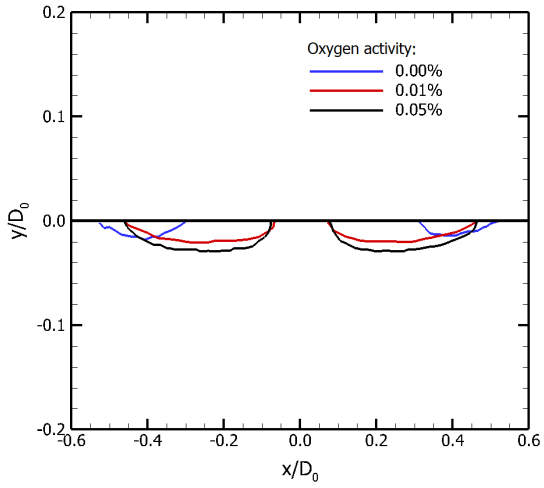

Figure A.1: Maximum cross sectional substrate melting after a molten droplet impinges on a cold substrate with different oxygen activity.

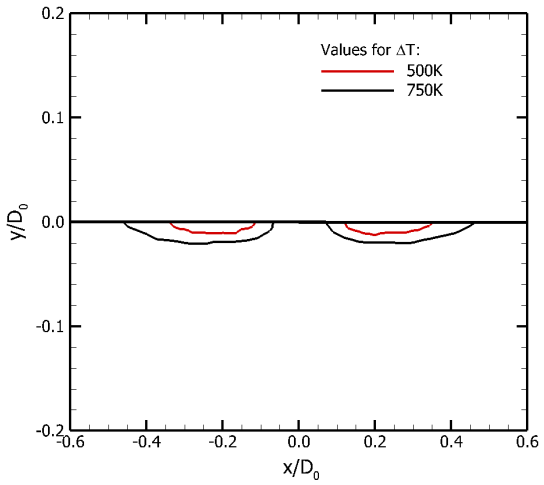

Figure A.2: Maximum cross sectional substrate melting after a molten droplet impinges on a cold substrate with different initial temperatures.

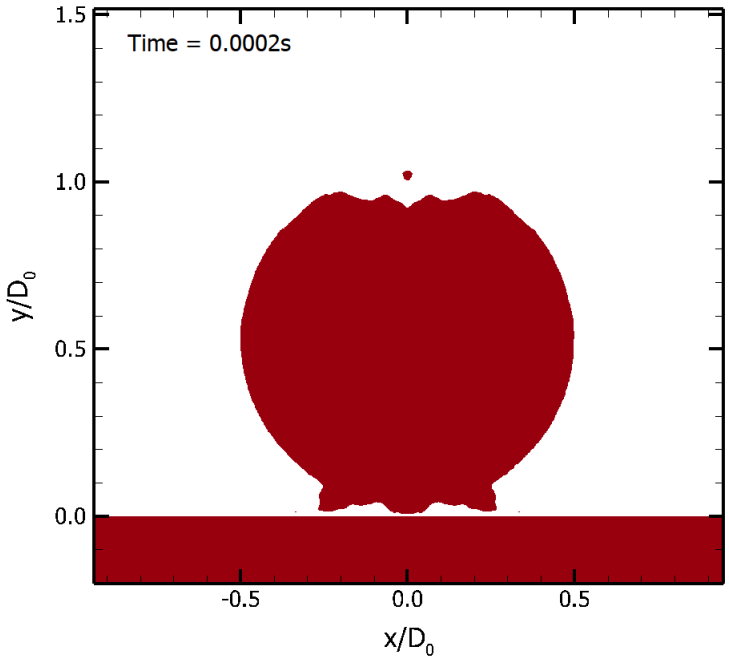

Figure A.3: Molten droplet impinging on a cold substrate with $\Delta T = 250$K. This figure shows the protrusion that traps air underneath the droplet.

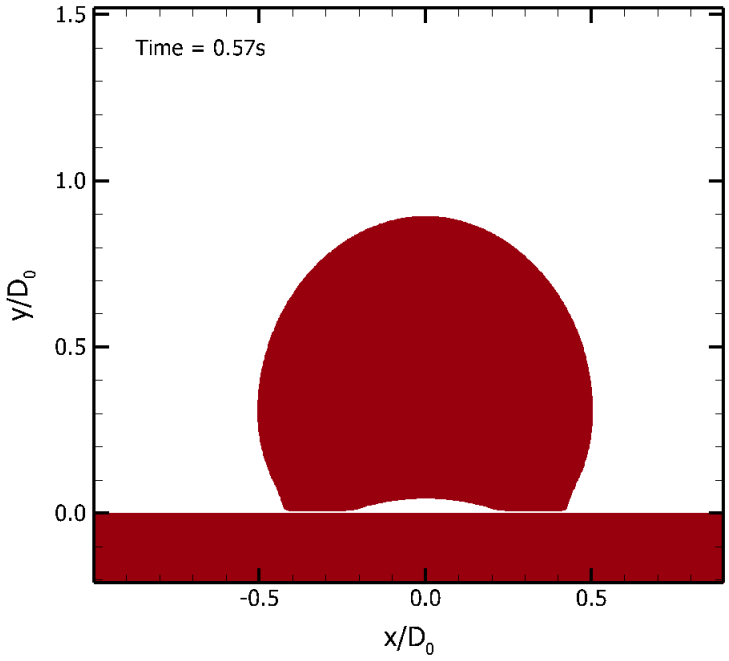

Figure A.4: Molten droplet impinging on a cold substrate with $\Delta T = 250$K. This figure shows the droplet after solidification and the air trapped underneath the droplet.

Bibliography

[1] S. Chandra and C. T. Avedisian, *On the collision of a droplet with a solid surface,* Proceedings of the Royal Society A: Mathematical, Physical and Engineering Sciences **432**, 13 (1991).

[2] M. Rein, *Phenomena of liquid drop impact on solid and liquid surfaces,* Fluid Dynamics Research **12**, 61 (1993).

[3] R. C. Dykhuizen, *Review of impact and solidification of molten thermal spray droplets,* Journal of Thermal Spray Technology **3**, 351 (1994).

[4] S. D. Aziz and S. Chandra, *Impact, recoil and splashing of molten metal droplets,* International Journal of Heat and Mass Transfer **43**, 2841 (2000).

[5] A. Yarin, *DROP IMPACT DYNAMICS: Splashing, spreading, receding, bouncing…,* Annual Review of Fluid Mechanics **38**, 159 (2006).

[6] S. Chandra and P. Fauchais, *Formation of solid splats during thermal spray deposition,* Journal of Thermal Spray Technology **18**, 148 (2009).

[7] C. Josserand and S. Thoroddsen, *Drop impact on a solid surface,* Annual Review of Fluid Mechanics **48**, 365 (2016).

[8] L. J. Zarzalejo, K. S. Schmaltz, and C. H. Amon, *Molten droplet solidification and substrate remelting in microcasting part i: numerical modeling and experimental verification,* Heat and Mass Transfer **34**, 477 (1999).

[9] K. S. Schmaltz, L. J. Zarzalejo, and C. H. Amon, *Molten droplet solidification and substrate remelting in microcasting part II: Parametric study and effect of dissimilar materials,* Heat and Mass Transfer **35**, 17 (1999).

[10] G. Trapaga, E. F. Matthys, J. J. Valencia, and J. Szekely, *Fluid flow, heat transfer, and solidification of molten metal droplets impinging on substrates: Comparison of numerical and experimental results,* Metallurgical Transactions B **23**, 701 (1992).

[11] D. Attinger and D. Poulikakos, *Melting and resolidification of a substrate caused by molten microdroplet impact,* Journal of Heat Transfer **123**, 1110 (2001).

[12] D. Attinger, Z. Zhao, and D. Poulikakos, *An experimental study of molten microdroplet surface deposition and solidification: Transient behavior and wetting angle dynamics,* Journal of Heat Transfer **122**, 544 (2000).

[13] F. H. Harlow and J. P. Shannon, *The splash of a liquid drop,* Journal of Applied Physics **38**, 3855 (1967).

[14] K. Tsurutani, M. Yao, J. Senda, and H. Fujimoto, *Numerical analysis of the deformation process of a droplet impinging upon a wall,* JSME international journal. Ser. 2, Fluids engineering, heat transfer, power, combustion, thermophysical properties **33**, 555 (1990).

[15] V. Butty, D. Poulikakos, and J. Giannakouros, *Three-dimensional presolidification heat transfer and fluid dynamics in molten microdroplet deposition,* International Journal of Heat and Fluid Flow **23**, 232 (2002).

[16] S. Ganesan, S. Rajasekaran, and L. Tobiska, *Numerical modeling of the non-isothermal liquid droplet impact on a hot solid substrate,* International Journal of Heat and Mass Transfer **78**, 670 (2014).

[17] C. Hirt and B. Nichols, *Volume of fluid (VOF) method for the dynamics of free boundaries,* Journal of Computational Physics **39**, 201 (1981).

[18] S. Osher and R. P. Fedkiw, *Level set methods: An overview and some recent results,* Journal of Computational Physics **169**, 463 (2001).

[19] M. Sussman, P. Smereka, and S. Osher, *A level set approach for computing solutions to incompressible two-phase flow,* Journal of Computational Physics **114**, 146 (1994).

[20] X. Zheng, J. Lowengrub, A. Anderson, and V. Cristini, *Adaptive unstructured volume remeshing – II: Application to two- and three-dimensional level-set simulations of multiphase flow,* Journal of Computational Physics **208**, 626 (2005).

[21] M. Pasandideh-Fard, Y. M. Qiao, S. Chandra, and J. Mostaghimi, *Capillary effects during droplet impact on a solid surface,* Physics of Fluids **8**, 650 (1996).

[22] M. Bussmann, J. Mostaghimi, and S. Chandra, *On a three-dimensional volume tracking model of droplet impact,* Physics of Fluids **11**, 1406 (1999).

[23] M. Pasandideh-Fard, S. Chandra, and J. Mostaghimi, *A three-dimensional model of droplet impact and solidification,* International Journal of Heat and Mass Transfer **45**, 2229 (2002).

[24] J. Madejski, *Solidification of droplets on a cold surface,* International Journal of Heat and Mass Transfer **19**, 1009 (1976).

[25] S. Kamnis and S. Gu, *Numerical modelling of droplet impingement,* Journal of Physics D: Applied Physics **38**, 3664 (2005).

[26] S. Haferl, V. Butty, D. Poulikakos, J. Giannakouros, K. Boomsma, C. Megaridis, and V. Nayagam, *Freezing dynamics of molten solder droplets impacting onto flat substrates in reduced gravity,* International Journal of Heat and Mass Transfer **44**, 3513 (2001).

[27] R. Monti, R. Savino, and S. Tempesta, *Wetting prevention by thermal marangoni effect. experimental and numerical simulation,* European Journal of Mechanics - B/Fluids **17**, 51 (1998).

[28] C. Cao, N. Wang, B. Wei, and H. De Groh, *Rapid solidification of ag-si eutectic alloys in drop tube, Progress in Natural Science*, **9**, 687 (1999).

[29] Y. Z. J. M. Khodadadi, *EFFECTS OF THERMOCAPILLARY CONVECTION ON MELTING WITHIN DROPLETS,* Numerical Heat Transfer, Part A: Applications **37**, 133 (2000).

[30] S. Song and B. Li, *Free surface profiles and thermal convection in electrostatically levitated droplets,* International Journal of Heat and Mass Transfer **43**, 3589 (2000).

[31] M. Dietzel, S. Haferl, Y. Ventikos, and D. Poulikakos, *Marangoni and variable viscosity phenomena in picoliter size solder droplet deposition,* Journal of Heat Transfer **125**, 365 (2003).

[32] R. J. Braun, B. T. Murray, W. J. Boettinger, and G. B. McFadden, *Lubrication theory for reactive spreading of a thin drop,* Physics of Fluids **7**, 1797 (1995).

[33] B. A. Nichita, *An improved CFD tool to simulate adiabatic and diabatic two-phase flows*, Ph.D. thesis, Swiss Federal Institue of Technology EPFL (2003).

[34] Y. Zhang, S. Matthews, A. Tran, and M. Hyland, *Effects of interfacial heat transfer, surface tension and contact angle on the formation of plasma-sprayed droplets through simulation study,* Surface and Coatings Technology **307**, 807 (2016).

[35] Y. Z. Zheng, Q. Li, Z. H. Zheng, J. F. Zhu, and P. L. Cao, *Modeling the impact, flattening and solidification of a molten droplet on a solid substrate during plasma spraying,* Applied Surface Science **317**, 526 (2014).

[36] G. R. Belton, *Langmuir adsorption, the gibbs adsorption isotherm, and interfacial kinetics in liquid metal systems,* Metallurgical and Materials Transactions B **7**, 35 (1976).

[37] P. Sahoo, T. Debroy, and M. J. McNallan, *Surface tension of binary metal—surface active solute systems under conditions relevant to welding metallurgy,* Metallurgical Transactions B **19**, 483 (1988).

[38] C. Zhao, C. Kwakernaak, Y. Pan, I. Richardson, Z. Saldi, S. Kenjeres, and C. Kleijn, *The effect of oxygen on transitional marangoni flow in laser spot welding,* Acta Materialia **58**, 6345 (2010).

[39] J. Brackbill, D. Kothe, and C. Zemach, *A continuum method for modeling surface tension,* Journal of Computational Physics **100**, 335 (1992).

[40] J. Straub, A. Weinzierl, and M. Zell, *Thermokapillare grenzflächenkonvektion an gasblasen in einem temperaturgradientenfeld,* Wärme- und Stoffübertragung **25**, 281 (1990).

[41] Z. S. Saldi, *Marangoni driven free surface flows in liquid weld pools*, Ph.D. thesis, Delft Univerisity of Technology (2012).

[42] P. V. Carey, *Liquid-Vapour Phase-Change Phenomena* (Taylor & Francis, 1992) Chap. 2.6.

[43] S. Y. Lee and S. U. Ryu, *Recent progress of spray-wall interaction research,* Journal of Mechanical Science and Technology **20**, 1101 (2006).

[44] A. Tomiyama, I. Zun, A. Sou, and T. Sakaguchi, *Numerical analysis of bubble motion with the VOF method,* Nuclear Engineering and Design **141**, 69 (1993).

[45] ANSYS, *ANSYS Fluent 12.0 User's Guide* (2009).

[46] M. Sussman, E. Fatemi, P. Smereka, and S. Osher, *An improved level set method for incompressible two-phase flows,* Computers & Fluids **27**, 663 (1998).

[47] E. Olsson, G. Kreiss, and S. Zahedi, *A conservative level set method for two phase flow II,* Journal of Computational Physics **225**, 785 (2007).

[48] S. Patankar and D. Spalding, *A calculation procedure for heat, mass and momentum transfer in three-dimensional parabolic flows,* International Journal of Heat and Mass Transfer **15**, 1787 (1972).

[49] A. Vorobyev, V. Kriventsev, and W. Maschek, *Simulation of central sloshing experiments with smoothed particle hydrodynamics (SPH) method,* Nuclear Engineering and Design **241**, 3086 (2011).

[50] J. C. Martin and W. J. Moyce, *Part IV. an experimental study of the collapse of liquid columns on a rigid horizontal plane,* Philosophical Transactions of the Royal Society A: Mathematical, Physical and Engineering Sciences **244**, 312 (1952).

[51] M. Ketabdari, M. Nobari, and M. M. Larmaei, *Simulation of waves group propagation and breaking in coastal zone using a navier–stokes solver with an improved VOF free surface treatment,* Applied Ocean Research **30**, 130 (2008).

[52] V. R. Voller and C. R. Swaminathan, *ERAL SOURCE-BASED METHOD FOR SOLIDIFICATION PHASE CHANGE,* Numerical Heat Transfer, Part B: Fundamentals **19**, 175 (1991).

[53] L. Tan, S. Leong, E. Leonardi, and T. Barber, *A numerical study of solid-liquid phase change with marangoni effects using a multiphase approach,* Progress in Computational Fluid Dynamics, An International Journal **6**, 304 (2006).

[54] A. Kidess, *Multiscale modeling of mesoscale phenomena in weld pools*, Ph.D. thesis, Delft University of Technology (2016).

[55] S. Alavi, M. Passandideh-Fard, and J. Mostaghimi, *Simulation of semi-molten particle impacts including heat transfer and phase change,* Journal of Thermal Spray Technology **21**, 1278 (2012).